



Power and thrust measurements of marine current turbines under various hydrodynamic flow conditions in a cavitation tunnel and a towing tank

A.S. Bahaj^{a,*}, A.F. Molland^b, J.R. Chaplin^a, W.M.J. Batten^a

^a*Sustainable Energy Research Group, School of Civil Engineering and the Environment,
University of Southampton, UK*

^b*School of Engineering Sciences, Ship Science, University of Southampton, UK*

Received 5 November 2005; accepted 31 January 2006

Available online 20 March 2006

Abstract

The results of cavitation tunnel and tank tests on an 800 mm diameter model of a marine current turbine (MCT) are presented. The tests were carried out in a 2.4 m × 1.2 m cavitation tunnel and the 60 m towing tank. Results for power and thrust coefficients are presented for a range of tip speed ratio and pitch settings for various conditions. The results of this investigation provided an insight into the operation of a single turbine in straight or yawed flow, the effect on performance of changes in the tip immersion of the rotor, the interference between twin rotors and the likely areas of cavitation inception. In addition, the analysed results presented provide useful information for the hydrodynamic design of MCTs and detailed data for the validation of numerical models.

© 2006 Elsevier Ltd. All rights reserved.

Keywords: Tidal stream; Marine currents; Marine current turbines; Tidal energy; Ocean energy; Turbine design

1. Introduction

There is a growing market for ‘green’ energy derived from sustainable resources throughout the world, with many countries offering incentives and targets. The oceans around the world offer a large energy source that is yet to be significantly tapped. Although the power from waves and ocean thermal currents are larger, tidal or marine currents with peak flows of over

*Corresponding author. Tel.: +44 23 80592051; fax: +44 23 80677519.

E-mail address: A.S.Bahaj@soton.ac.uk (A.S. Bahaj).

Nomenclature

A	rotor area (m^2)
c	blade chord (m)
C_p	pressure coefficient
C_P	power coefficient
C_T	thrust coefficient
D	rotor diameter (m)
g	gap between rotor tips (m)
P_T	tunnel pressure (static + gravity) (N/m^2)
P_V	water vapour pressure (assumed $2000 \text{ N}/\text{m}^2$)
Q	rotor torque (N m)
R	blade tip radius (m)
t	blade thickness (m)
T	rotor thrust (N)
TSR	Tip Speed Ratio ($\Omega R/U$)
U	flow speed (m/s)
U_T	tunnel speed or test tank carriage speed (m/s)
U_F	free stream speed or test tank carriage speed (m/s)
V	reference velocity (m/s)
γ	yaw angle (degrees)
ρ	fluid density (kg/m^3)
σ	cavitation number
Ω	rotational speed of rotor (rad/s)

four knots, caused by constrained topography, offer an exciting proposition for the extraction of predictable energy. Many devices are being studied for marine current energy conversion although most are designed around horizontal axis turbines, known as a marine current turbine (MCT) [1,2]. One possible site for MCTs is the Race of Alderney in the Channel Islands [3,4], which could supply as much as 1.34 TWh/year with large farm of MCTs.

In addition, there is now a concerted effort to progress tidal energy technologies through nationally funded programmes throughout the UK. It is therefore important to be able to predict energy yields for this technology which will allow appropriate designs to be qualified and validated. To this end, methodologies need to be established which will describe the physical and operational performance of the turbines, allowing their design to be investigated and performance evaluated.

Much can be transferred from the design and operation of wind turbines [5]. There are however a number of fundamental differences in the design and operation which will require further investigation, research and development. Particular differences entail changes in Reynolds number, different stall characteristics and the possible occurrence of cavitation. However, there is a wealth of information available on the cavitation and stall characteristics of marine propellers [6], which can provide a useful starting point for the investigation of MCTs.

The work presented here describes the design of a rig to test models of MCTs and the experimental measurements which were carried out in both a cavitation tunnel and a test tank. The objectives of the tests were to obtain the characteristics of turbine power and thrust

for a range of rpm, flow speed and hub pitch angle. The secondary effects of rotor depth, yaw and dual rotor interference were also studied. Further details of the tests are given in [7] including tables of results. These secondary effects are important when designing a MCT to match a site as the tidal depth governs the size of the turbine and the shape of the tidal ellipse defines the possibility and amount of yawed flow that may be present on the rotor.

The work described also forms a part of a wider research programme, which included the development of a theoretical model of the performance characteristics of MCTs [8–11].

2. Test facilities

2.1. Cavitation tunnel

The tests were carried out in the cavitation tunnel at QinetiQ, Haslar, Gosport, which has the following working section particulars:

Length	5 m
Breadth	2.4 m
Height	1.2 m
Max flow speed	8 m/s
Pressure range	0.2–1.2 atm

The tunnel is fully enclosed and the speed was measured using a pitot-static tube. Tunnel static pressures were measured on the sidewall of the working section. The accuracy of tunnel speed and pressure is estimated to be within 1%.

2.2. Test tank

Tests were carried out in the Towing Tank at Southampton Institute, which has the following working section particulars:

Length	60 m
Breadth	3.7 m
Depth	1.8 m
Maximum carriage speed	4.5 m/s

The tank has a manned carriage which is equipped with a dynamometer for measuring model forces with various computer and instrumentation facilities for automated data acquisition. The test rig was instead mounted from a pair of aluminium channel beams mounted aft of the carriage. The carriage-based computer equipment was used to log the carriage speed. The accuracy of carriage speed is estimated to be within 1%.

3. Description of models

3.1. Blades and hub

A rotor diameter of 800 mm was chosen as a compromise between maximising Reynolds number and not incurring excessive tunnel blockage correction. The boss diameter to suit

Table 1
Particulars of turbine blades and hub

r/R	Radius (mm)	c/R	Pitch distribution (deg)	t/c (%)
0.2	80	0.125	15	24
0.25	100	0.1203	12.1	22.5
0.3	120	0.1156	9.5	20.7
0.35	140	0.1109	7.6	19.5
0.4	160	0.1063	6.1	18.7
0.45	180	0.1016	4.9	18.1
0.5	200	0.0969	3.9	17.6
0.55	220	0.0922	3.1	17.1
0.6	240	0.0875	2.4	16.6
0.65	260	0.0828	1.9	16.1
0.7	280	0.0781	1.5	15.6
0.75	300	0.0734	1.2	15.1
0.8	320	0.0688	0.9	14.6
0.85	340	0.0641	0.6	14.1
0.9	360	0.0594	0.4	13.6
0.95	380	0.0547	0.2	13.1
1.0	400	0.05	0	12.6

the test rig was 100 mm. The blades were developed from the profile shape of a NACA 63-8xx and a chord, thickness and pitch distribution as shown in Table 1.

The model blades were manufactured from 3D model drawings derived from 2D section coordinates interpolated from coordinate-based data for NACA 63-812, 63-815, 63-818, 63-821 and 638-24 for 17 stations along the blade. The blades were machined from T6082-T6 aluminium alloy on a 5-axis computer numerical control (CNC) machine at the University of Southampton to an order of accuracy of ± 0.05 mm. They are then brought to a smooth hydrodynamic finish and anodised for protection.

The layout of the blades and hub is shown in Fig. 1. This shows details of the geometry of the blade root that is clamped in the hub. The rotor hub consists of three parts, the front cone and the two halves that clamp the blades. This allows any pitch angle to be set. For this series of tests the hub pitch angle refers to the nose-tail angle of the blade at a radius of 80 mm ($0.2R$). The blade pitch angle was measured using a digital inclinometer resting on a template that sits on the blade at a radius of 80 mm. The datum surface of the inclinometer is at the same angle as the tip; this is then converted to the blade pitch angle at 80 mm radius.

4. Test rig

4.1. Design and test requirements

The instrumented test rig was designed to incorporate the following features:

- a dynamometer to allow measurements of torque and thrust in the turbine hub before any bearing or seal losses;
- a split rotor hub to allow easy changes of rotor blades and blade pitch angles;



Fig. 1. Photograph of the blade and hub components.

- to withstand the water pressure and the vacuum pressure in the cavitation tunnel;
- the upright support to be at least one rotor radius downstream of the rotor in order to minimise the effect on its performance;
- the horizontal main body to have a diameter no larger than that of the hub.

4.2. Test rig layout

The experimental rig consists of a three-bladed rotor attached to a main shaft which drives a generator from a pulley through a belt carried up through the vertical support tube. The rig can accommodate model rotors up to about 900 mm. The choice of a timing belt drive system enabled a slender main body, the size of the rotor hub, to be used and a similar size of vertical support tube. The overall concept of the model in the cavitation tunnel is shown in Fig. 2. More details of the layout including the rotor hub, dynamometer, slip rings, pulleys and bearings are shown in Fig. 3.

4.3. Hub dynamometer

An in-line strain gauge dynamometer mounted next to the turbine rotor, and running wet, was used to measure the thrust and torque. The dynamometer, seals and rig have to withstand a pressure head above atmospheric at the deepest position in the towing tank, of $116 \times 10^3 \text{ N/m}^2$ and a reduction (vacuum) below atmospheric of $21 \times 10^3 \text{ N/m}^2$ during cavitation tests.

The dynamometer has the capability of measuring 1000 N of thrust and 50 N m. The layout of the dynamometer is similar to [11], photographs are shown in Fig. 4 and detailed drawings are presented in [7]. The dynamometer is wired in a full bridge circuit with two Vishay transducer linear single grid (J2A-06-S110k-10C) gauges on each bridge arm. The wires from the gauges are run through a watertight seal into the hollow shaft and then via a slip-ring assembly to bridge conditioners.

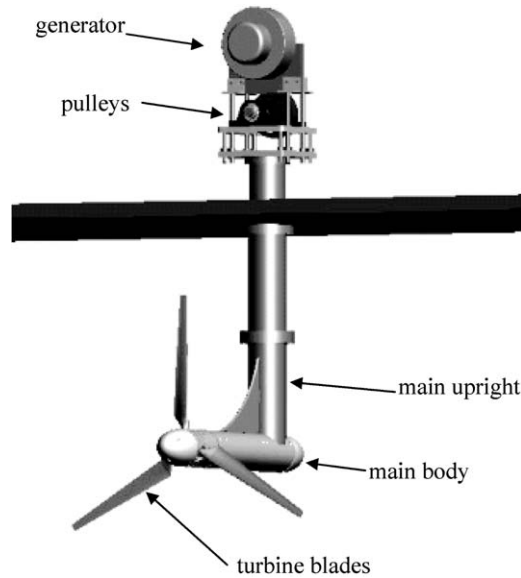


Fig. 2. Visualisation of the experimental rig in the cavitation tunnel.

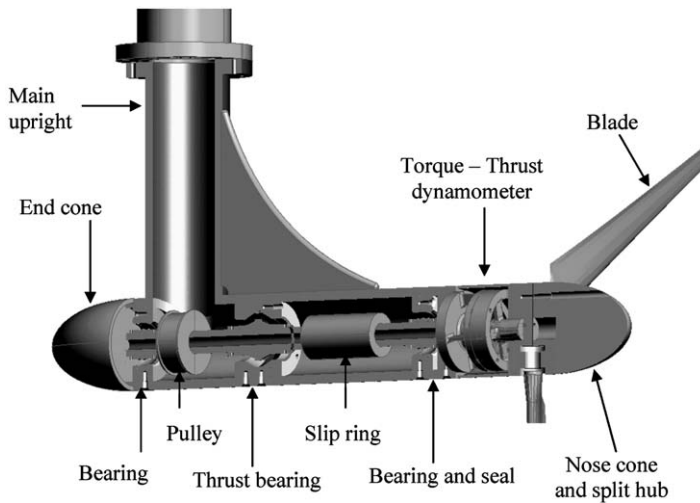


Fig. 3. Cross section of the experimental rig showing key components.

The responses were recorded directly from a voltmeter, amplified and acquired on a computer. The dynamometer was calibrated fully wired with slip rings in place before and after testing. Results of the calibrations are given in [7]. The torque can be measured to within ± 0.25 N m and the thrust to within ± 5 N. Based upon a flow speed of 1.5 m/s and using typical coefficients of $C_P = 0.4$ and $C_T = 0.8$, leads to an accuracy of the order of 71.3% for power and 71.1% for thrust.



Fig. 4. Details of the assembled torque/thrust dynamotor showing geometry and sealing. (a) CAD model, (b) upstream photograph, (c) downstream photograph.

4.4. Power control

The power is absorbed via a belt drive system to a DC generator (up to 10 kW) connected to rheostats. The speed of the rotor for a given tunnel speed was regulated by altering the loading of the rheostats. Up to three $1.5\ \Omega/25\ \text{A}$ rheostats were wired in parallel to improve the sensitivity of the control and reduce the current. The rotor RPM was measured optically using a tachometer.

4.5. Data acquisition system

Stabilised bridge voltages and bridge conditioning for the thrust/torque dynamometer were provided by a Fylde box. Output signals from the dynamometer, together with rotor revs, were acquired using an A/D card and a laptop computer. The water flow speed was acquired separately using the tunnel and test tank systems.

5. Test programme

5.1. Overview

The objectives of the tests were to derive a reliable set of MCT performance characteristics under controlled conditions. This would entail the measurement of power and thrust performance characteristics over a range of flow speed, rotor revolutions and rotor blade pitch settings. The cavitation inception test would also involve reduced tunnel pressures to simulate cavitating conditions.

5.2. Cavitation tunnel

The 800 mm diameter rotor was arranged to be close to the centre of the tunnel, as shown in Fig. 5. Over the five days of testing, five hub pitch angles ranging from 15° to 30° were tested at tunnel speeds ranging from 0.8 to 2.0 m/s. The range of required tip speed ratios (TSRs) required for this investigation was achieved with constant tunnel speed by varying the rotor RPM. The variation in rotor RPM was achieved by varying the load on the rheostats. For the cavitation inception tests, the water speed and working section pressure were set at the required values. The turbine RPM was increased or decreased until cavitation was visible. The cavitation was observed under a strong light and a video recorded. This was carried out for two pitch angles of 20° and 25° .

5.3. Towing tank

The rig was set up in the tank with a tip immersion of 150 mm ($0.19D$) followed by a tip immersion of 440 mm ($0.55D$), as shown in Fig. 6. Tests were carried out at speeds ranging from 0.8 to 1.5 m/s and yaw angles from 0° to 30° . A further identical dummy rotor

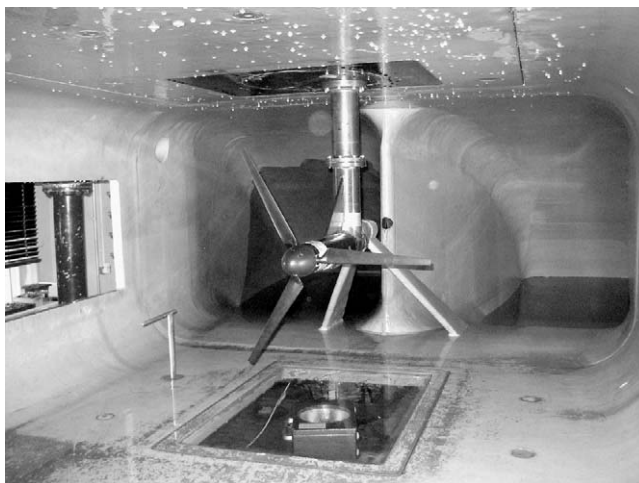


Fig. 5. Photograph of the assembled test rig in the cavitation tunnel.

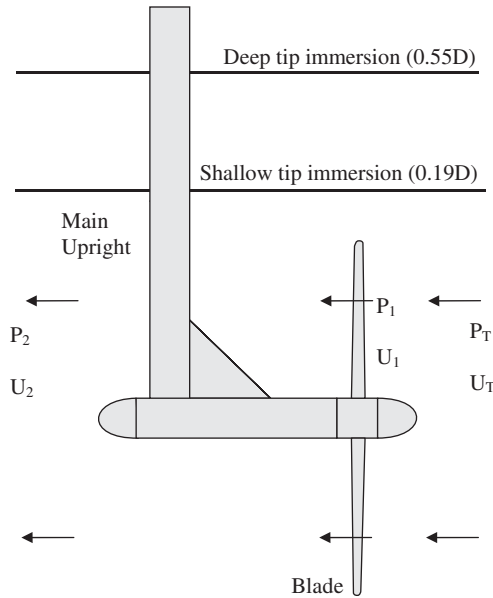


Fig. 6. Effect of depth of immersion on the rotor.

(not instrumented) was introduced and twin rotor tests were carried out for different TSR values and different separations of the rotors.

6. Data reduction and presentation

6.1. General

For a given tunnel flow speed and rotational speed, the torque and the thrust were acquired from the dynamometer. The averaged excitation voltages from the torque and thrust bridge circuits were corrected for zero offset and then multiplied by the calibration factor to resolve the torque (Q) and thrust (T). The TSR, power (C_P) and thrust (C_T) coefficients were non-dimensionalised in the following way:

$$\text{Tip Speed Ratio : } \text{TSR} = \frac{\Omega R}{U_T}, \quad (1)$$

$$\text{Power coefficient : } C_P = \frac{Q\Omega R}{(1/2)\rho U_T^3 A}, \quad (2)$$

$$\text{Thrust coefficient : } C_T = \frac{T}{(1/2)\rho U_T^2 A}, \quad (3)$$

$$\text{Cavitation Number : } \sigma = \frac{P_T - P_V}{(1/2)\rho V^2}. \quad (4)$$

The reference velocity was taken to be the velocity at the blade tip: $V = \sqrt{U_T^2 + \Omega^2 R^2}$.

6.2. Blockage correction

The normal boundary corrections for propellers, e.g., Glauert [12] or Pope and Harper [13] are not suitable for negative thrust (effectively the case of a generating turbine). In order to correct for blockage, Glauert's equations have been modified for wake expansion in the case of a turbine by Barnsley and Wellicome [14]. The method is based on an actuator disc model of the flow through the turbine in which the flow is presumed to be uniform across any cross section of the stream tube enclosing the turbine disc. A discontinuity of pressure is presumed across the disc, directly related to the turbine thrust load. The equations are presented in Appendix A and are used to correct for boundary effects to present results based on free stream inflow speed. For example, with a single rotor and a thrust coefficient of 0.8, the corrections amounted up to 18% decrease in power coefficient and 11% decrease in thrust coefficient for the cavitation tunnel and up to 8% and 5% decrease, respectively, for the towing tank.

6.3. Presentation

The results are graphically presented in Figs. 7–11. Tables 2 and 3 tabulate the results of the twin rotor tests. Notes on cavitation inception are presented in Tables 4 and 5 and in the photograph sequence in Fig. 12.

7. Results and discussion

7.1. Experiments

The results for the power and thrust coefficients (C_P and C_T), to a base of TSR, for the single rotor in the cavitation tunnel at zero yaw are shown in Fig. 6. The results are consistent and show an increase in C_P and C_T as hub pitch angle is reduced, with maximum $C_P = 0.46$ occurring for the design 20° pitch angle. The 20° hub pitch case showed the most consistent set of data. At higher pitch angles and lower loadings there is a little more scatter in the data.

Figs. 8 and 9 compare the results from the test tank and cavitation tunnel for hub pitch angles of 20° and 25° . In these figures, for clarity of presentation, the upper diagrams show the data points and curve fits and the lower diagrams the comparison of these same curve fits. In Fig. 8 it is noted that there is little difference between the results from the cavitation tunnel at the two speeds of 1.0 and 1.7 m/s. It is also seen that the test tank results for the deep tip-immersion ($h = 0.55D$) are similar to the cavitation tunnel results except at low TSR when they are a little lower. This result is reassuring and confirms the viability of using both facilities for such tests.

The power coefficient results for the test tank with shallow tip-immersion ($h = 0.19D$) are 10–15%, lower than the deep immersion results, Figs. 8 and 9. The thrust results for the shallow tip-immersion case are about 5% lower than the deep tip-immersion case. This significant reduction in power and decrease in thrust arises due to the proximity of the free surface, with the rotor tip immersion being only 19% of the rotor diameter.

The proximity of the free surface, Fig. 6, acting like a reflection plane will tend to prevent the full expansion of the wake. This causes a reduction in the pressure difference across the turbine, causing a reduction in both the power and thrust produced. However,

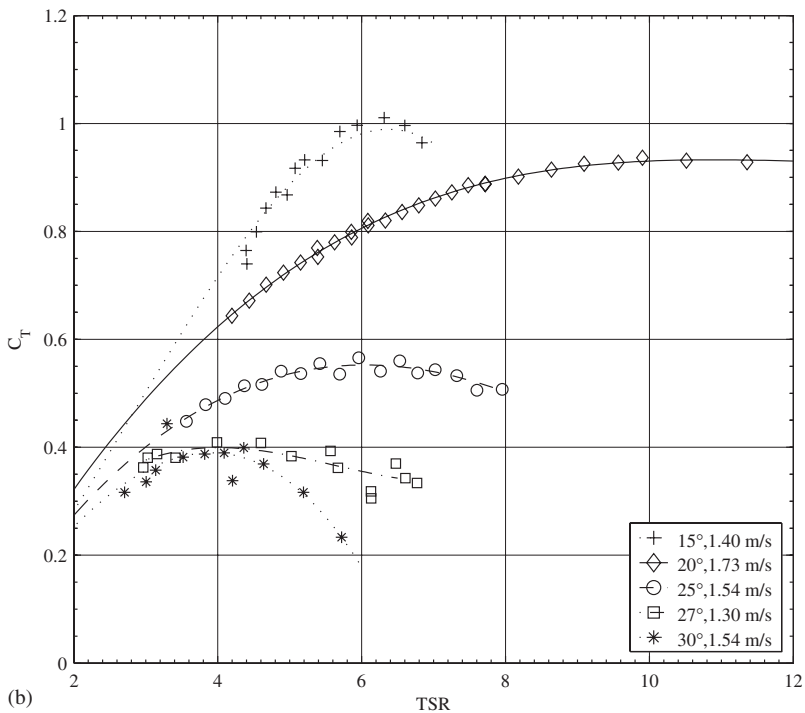
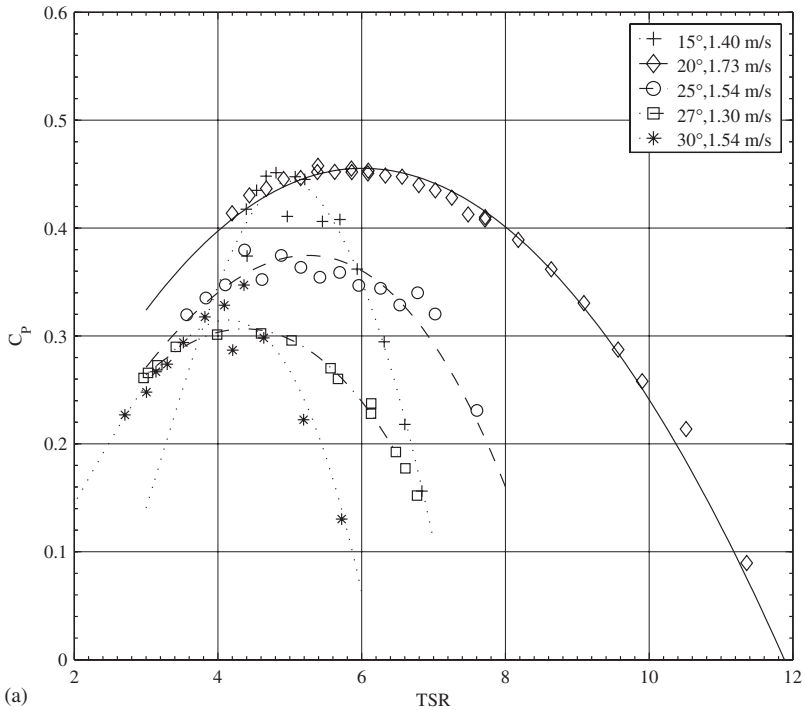


Fig. 7. Comparisons of hub at pitch angles at the cavitation tunnel—zero yaw. (a) Power coefficient, C_p , (b) thrust coefficient, C_T .

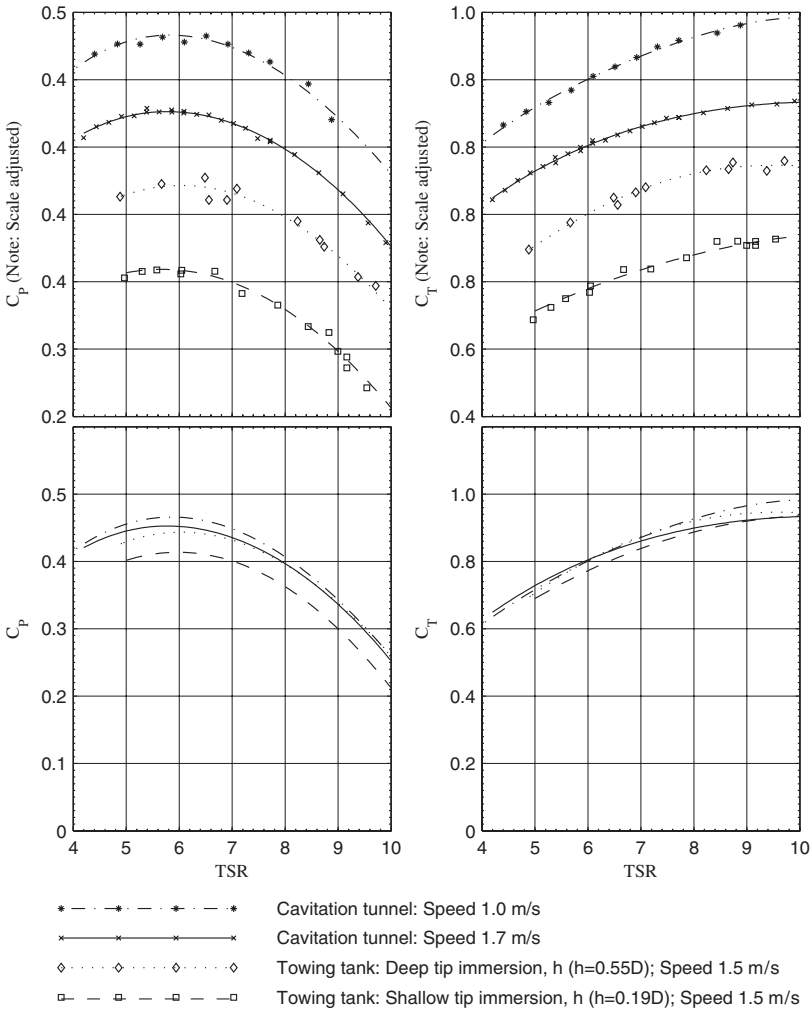


Fig. 8. Test tank vs cavitation tunnel—20° hub pitch angle.

the proximity of the free surface causes further losses arising from the creation of waves and this would account for an increase in thrust. Due to the summation of these factors, little change in thrust occurs for the shallow tip-immersion case, but a relatively large reduction in power is caused, as observed.

The influence of inflow yaw angle on rotor performance, as tested in the towing tank, is shown in Figs. 10 and 11 for hub pitch angles of 20° and 25°. Both cases show a consistent decrease in power and thrust with increasing yaw angle. Power tends to decrease approximately as a function of the cosine of the yaw angle squared and thrust as cosine of the yaw angle [5]. For example, for both the 20° and 25° hub pitch angles, a 30° yaw angle reduced the power coefficient by about 30%, whilst the thrust coefficient was reduced by about 15% for the 20° pitch angle and 25% for the 25° pitch angle.

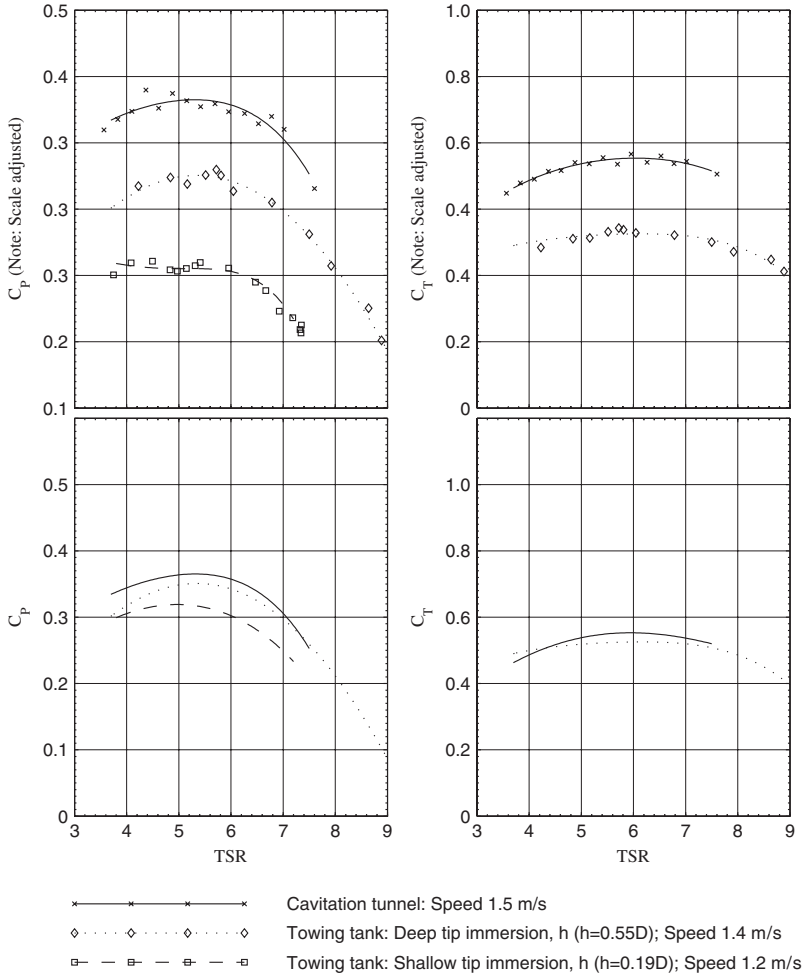


Fig. 9. Tank vs cavitation tunnel at 25° hub pitch angle.

The results for the dual rotor tests are given in Tables 2 and 3. As the results showed relatively small changes, plots of the data were difficult to interpret and are therefore not included. The tests were carried out in the test tank and the deep tip-immersion ($h = 0.55D$) was used. Cases were run with the second (identical dummy) rotor static and rotating. When rotating, the dummy rotor was not necessarily running at the same TSR (rpm) as the main (instrumented) rotor, as shown in Table 2. Extra blockage corrections were applied when the dummy rotor was rotating.

It is seen from Table 2, that whether the dummy second rotor is static or rotating at speeds at or different to the main rotor, it has very little influence on the performance of the main rotor. Table 3 gives a summary (interpolated for $TSR = 7$) of the effect of horizontal gap clearance between the two rotors on the power and thrust coefficients. It is seen that even at extremely small gaps, any interference effects were very small and not measurable.

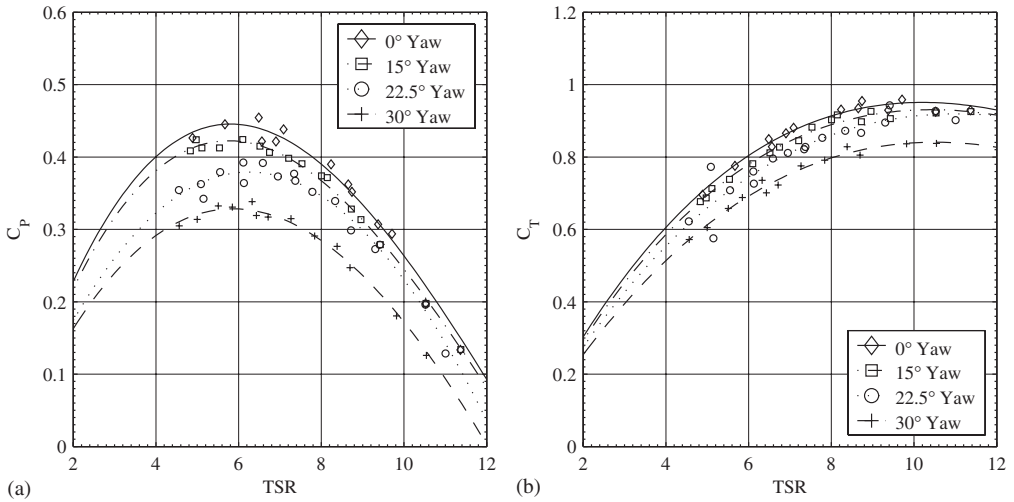


Fig. 10. Comparison of the effect of yaw with 20° hub pitch at towed speed of 1.4 m/s. (a) Power coefficient (C_p), (b) thrust coefficient (C_T).

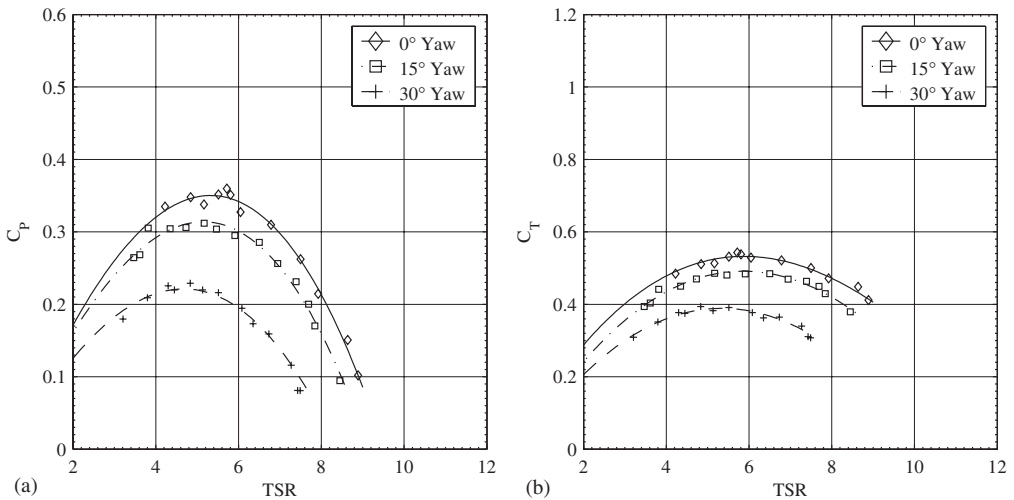


Fig. 11. Comparison of the effect of yaw with 25° hub pitch at towed speed of 1.4 m/s. (a) Power coefficient (C_p), (b) thrust coefficient (C_T).

A summary of the results of the cavitation inception investigation is given in Tables 4 and 5 and photographs showing the appearance of cavitation are given in Fig. 12. It is seen from Table 4 (25° hub pitch) and Fig. 12 that cavitation does not appear until the cavitation number, σ , has been reduced to about 0.9. When the cavitation number is reduced to below about 0.4, there is cavitation on the suction side over about 10–15% of the outer part of the blade. It is interesting to note in Fig. 11f the occurrence of a

Table 2
Effect of dummy TSR on power and thrust coefficient

g/R	Gap (mm)	TSR (rig)	TSR (dummy)	C_P	C_T		
0.25	100	6.6 ± 0.1	0	0.42	0.84		
		6.6 ± 0.1	6.5	0.43	0.83		
		6.6 ± 0.1	7.8	0.44	0.84		
		9.4 ± 0.1	0	0.32	0.94		
		9.4 ± 0.1	7.1	0.30	0.95		
		9.4 ± 0.1	8.6	0.30	0.95		
		9.4 ± 0.1	10.3	0.30	0.94		
		0.5	200	6.8 ± 0.1	0	0.43	0.8
				6.8 ± 0.1	5.2	0.41	0.82
				6.8 ± 0.1	7.6	0.42	0.81
6.8 ± 0.1	9.74			0.41	0.85		
8.8 ± 0.1	0			0.32	0.93		
8.8 ± 0.1	7.7			0.27	0.94		
8.8 ± 0.1	8.4			0.26	0.95		
8.8 ± 0.1	9.7			0.26	0.95		
1.0	400			7.4 ± 0.1	0	0.41	0.86
				7.4 ± 0.1	6.2	0.42	0.86
		7.4 ± 0.1	7.1	0.42	0.88		
		7.4 ± 0.1	9.1	0.42	0.87		

Table 3
Effect of gap width on power and thrust coefficient interpolated at TSR = 7

g/R	Gap (mm)	C_P (static)	C_P (rotating)	C_T (static)	C_T (rotating)
0.025	10	0.42	0.40	0.88	0.86
0.0625	25	0.42	0.42	0.88	0.88
0.125	50	0.41	0.40	0.88	0.86
0.25	100	0.42	0.41	0.89	0.88
0.375	150	0.42	0.41	0.88	0.87
0.5	200	0.42	0.41	0.86	0.88
1.0	400	0.41	0.42	0.88	0.89

Table 4
Cavitation observations with 25° hub pitch, $U_T = 1.4$ m/s

Static pressure (N/m ²)	rpm	TSR	V (m/s)	σ	Tip vortex cavitation	Blade cavitation
61,400	274	8.2	11.6	1.10	Detached vortex	—
32,000	272	8.1	11.5	0.67	Attached vortex	Cavitation mid-chord for 10% of blade
23,000	250	7.5	10.6	0.63	Attached vortex	Cavitation over 15% of the blade
21,000	240	7.2	10.2	0.64	Attached vortex	About the same amount of cavitation

Table 5
Cavitation observations with 20° hub pitch, $U_T = 1.4$ m/s

Static pressure (N/m ²)	rpm	TSR	V (m/s)	σ	Tip vortex cavitation	Blade cavitation
50,000	200	6.0	8.5	1.72	None	—
50,000	273	8.2	11.5	0.89	First appearance	—
31,000	300	9.0	12.6	0.54	Attached vortex	—
24,000	295	8.8	12.4	0.47	Attached vortex	Intermittent on blades
21,000	290	8.7	12.2	0.44	Attached vortex	Stronger cavitation at top 10–20% of blade

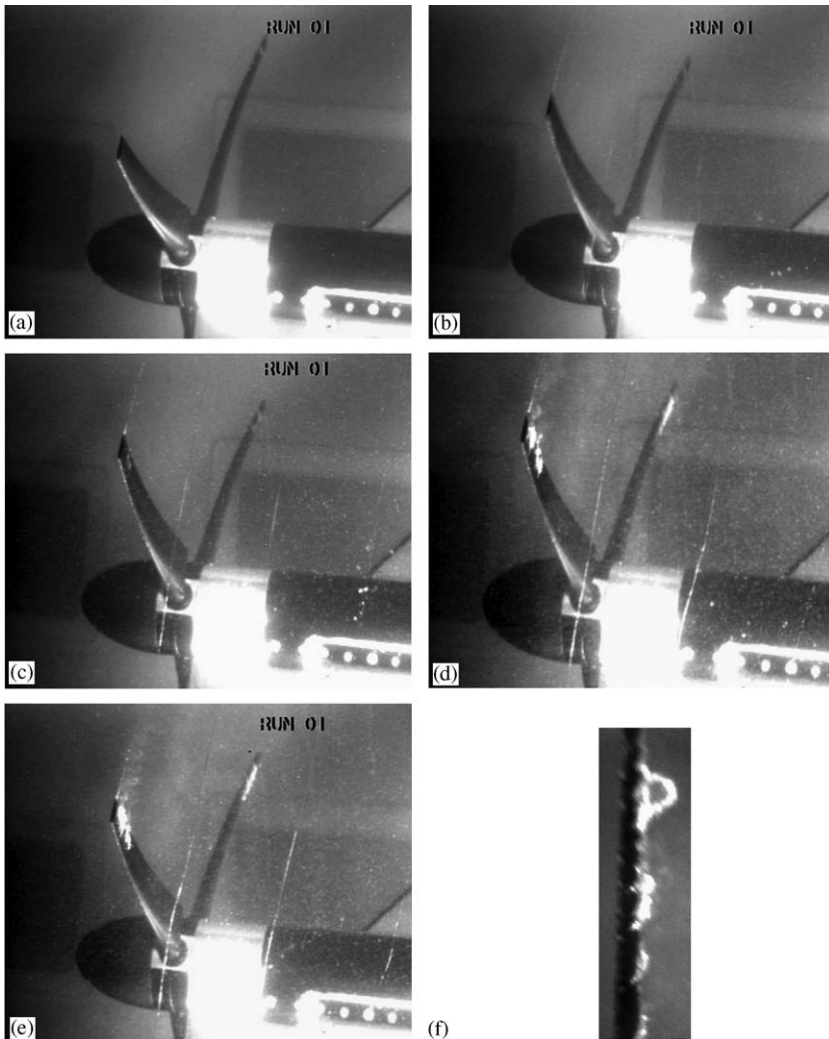


Fig. 12. Cavitation images with a 25° hub pitch at a flow speed of 1.4 m/s. (a) TSR = 8.2, $\sigma = 1.2$, (b) TSR = 8.2, $\sigma = 1.10$, (c) TSR = 8.1, $\sigma = 0.67$, (d) TSR = 7.2, $\sigma = 0.63$, (e) TSR = 7.5, $\sigma = 0.64$, (f) close up showing 'horseshoe' cavitation.

‘horseshoe’ cavitation structure as reported in [15]. Cavitation typically appears at TSR values greater than about 7.0, which, from Fig. 6, indicates a very high thrust loading. Similar deductions can be made for the 20° hub pitch angle, Table 5. These cavitation inception values correspond to the extreme left-hand end (low σ) of the cavitation inception envelope for this blade section, reported in [16] where, for the NACA 63-815 section, back bubble cavitation was observed. It can also be observed that these cavitation numbers at inception are generally below the cavitation numbers to be expected full-scale which might typically range from 1.5 to 6.0.

7.2. Implications for marine current turbines

1. The basic performance characteristics, Fig. 6, provide the areas of operation of MCTs for the maximum extraction of energy. In this configuration, it is indicated that TSR values of 5–7 and hub pitch angles of about 20° are the most suitable.
2. There are significant reductions in extracted power when the turbine is in a yawed condition, Figs. 7 and 8. This has to be taken into account when matching designs with tidal current characteristics for a particular site.
3. Significant reductions in extracted power were observed when the turbine tip immersion was reduced. This has implications for matching of rotor diameter to a particular depth of water.
4. No significant interference effects were observed when two rotors were run in close proximity. This should allow dual rotor system to be employed without significant loss in performance.
5. The investigation has indicated that with careful design of blade angles and tip speeds, it should be possible to prevent cavitation on full scale MCTs.

8. Conclusions

1. A rig has been designed, built and commissioned which has proved successful in measuring the performance characteristics of models of MCTs in a test tank and a cavitation tunnel.
2. The results of the investigations provide an insight into the operation of a single turbine in straight or yawed inflow, the effect on performance of changes in the tip immersion of the rotor, the interference between twin rotors and the likely areas of cavitation inception.
3. The results suggest that for deep water immersion MCTs the use of a solid wall cavitation tunnel is applicable.
4. Overall, a consistent set of experimental data have been produced which provide useful design information in their own right and suitable data for validating theoretical and numerical methods.

Acknowledgement

The work described in this paper covers part of a research project funded by the Engineering and Physical Science Research Council (EPSRC), grant GR/R50424/01.

Appendix A. Tunnel blockage correction

The blockage correction for wake expansion is based on an actuator disc model of the flow through the turbine in which the flow is presumed to be uniform across any cross section of the stream tube enclosing the turbine disc. A discontinuity of pressure is presumed across the disc, directly related to the turbine thrust load. This layout is shown in Fig. A1. Plane A is far enough upstream and Plane B far enough downstream of the disc for pressures to be uniform across the tunnel or tank cross section at these two planes. The subscripts T and F denote tunnel and free stream conditions, respectively.

Applying the principles of continuity and a momentum/force balance on the water between planes A and B the following relations are obtained between various velocities and the ratio of the disc area (*A*) to tunnel area (*C*):

$$\frac{U_1}{U_2} = \frac{-1 + \sqrt{1 + (A/C)((U_3/U_2)^2 - 1)}}{(A/C)((U_3/U_2) - 1)} \tag{A.1}$$

and

$$\frac{U_T}{U_2} = \frac{U_3}{U_2} - \frac{A U_1}{C U_2} \left[\frac{U_3}{U_2} - 1 \right]. \tag{A.2}$$

Whilst the turbine thrust is obtained non-dimensionally as

$$C_{T_T} = \frac{T}{0.5\rho A U_T^2} = \left(\frac{U_2}{U_T} \right)^2 \left[\left(\frac{U_3}{U_2} \right)^2 - 1 \right] \tag{A.3}$$

rearranged as

$$\frac{U_T}{U_2} = 1 / \sqrt{\frac{C_T}{\left[(U_3/U_2)^2 - 1 \right]}}. \tag{A.4}$$

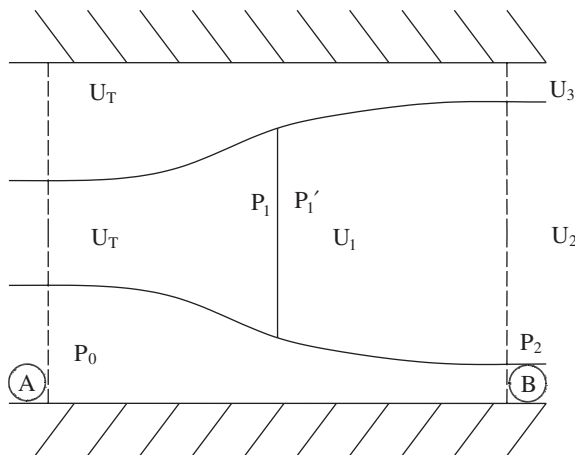


Fig. A1.

Assuming a range of values of U_3/U_2 , these equations can be solved by iteration such that the values of U_T/U_2 obtained from separate Eqs. (A.2) and (A.3) are equal. U_1/U_T can then be obtained as the product of U_1/U_2 from Eq. (A.1) and U_2/U_0 from Eq. (A.4).

To identify “equivalent open water” operating conditions the principle adopted is that the turbine blades will be operating at equivalent angles of attack and other equivalent conditions, if (a) the disc flow speed U_1 , (b) the turbine RPM and (c) the turbine thrust T , are the same in open water as in the tunnel test state. This leads to an equivalent water speed U_F given by

$$\frac{U_T}{U_F} = \frac{U_1/U_T}{(U_1/U_T)^2 + C_{T_T}/4}. \quad (\text{A.5})$$

This can be rearranged as the following wake blockage:

$$\varepsilon_{wb} = \frac{U_1}{U_T} + \frac{U_T}{U_1} \left(\frac{C_{T_T}}{4} - 1 \right). \quad (\text{A.6})$$

Based upon these blockage factors the increase in tunnel speed can be calculated and consequently the following corrections to the TSR, power and thrust non-dimensional coefficients were applied:

$$C_{PF} = C_{PF} \left(\frac{U_T}{U_F} \right)^3, \quad (\text{A.7})$$

$$C_{TF} = C_{TF} \left(\frac{U_T}{U_F} \right)^2, \quad (\text{A.8})$$

$$\text{TSR}_F = \text{TSR}_T \left(\frac{U_T}{U_F} \right). \quad (\text{A.9})$$

References

- [1] Fraenkel PL. Power from marine turbines. *Proc Inst Mech Eng A: J Power Energy* 2002;216(A1):1–14.
- [2] European Commission. The exploitation of tidal marine currents. Report EUR16683EN, 1996.
- [3] Bahaj AS, Myers LE. Analytical estimates of the energy yield potential from the Alderney Race (Channel Islands) using MCTs. *Renew Energy* 2004;29(12):1931–45.
- [4] Myers LE, Bahaj AS. Simulated electrical power potential harnessed by marine current turbine arrays in the Alderney Race. *Renew Energy* 2005;30(11):1713–31.
- [5] Burton T, Sharpe D, Jenkins N, Bossanyi E. *Wind energy handbook*. New York: Wiley; 2000.
- [6] Carlton JS. *Marine propellers and propulsion*. London: Butterworth Heinemann; 1994.
- [7] Bahaj AS, Batten WMJ, Molland AF, Chaplin JR. Experimental investigation into the hydrodynamic performance of marine current turbines. Sustainable energy series, Report 3, University of Southampton, March 2005.
- [8] Bahaj AS, Batten WMJ, Molland AF, Chaplin JR. Theoretical predictions of the hydrodynamic performance of marine current turbines. Sustainable energy series, Report 4, University of Southampton, March 2005.
- [9] Batten WMJ, Bahaj AS, Molland AF, Chaplin JR. Experimentally validated numerical method for the hydrodynamic design of horizontal axis tidal turbines. In: *Proceedings of sixth European wave and tidal energy conference—Glasgow, 29th Sept–2nd Oct 2005*.
- [10] Batten WMJ, Bahaj AS, Molland AF, Chaplin JR. Hydrodynamics of marine current turbines. *Renew Energy* 2006;31(2):249–56.

- [11] Molland AF, Turnock SR. A Propeller thrust and torque dynamometer for wind tunnel models. *Strain, J Br Soc Strain Meas* 2002;38(1):1.
- [12] Glauert H. The elements of aerofoil and airscrew theory, 2nd ed. New York: Cambridge University Press; 1947.
- [13] Pope A, Harper JJ. Low-speed wind tunnel testing, 2nd ed. New York: Wiley; 1966.
- [14] Barnsley MJ, Wellicome JF. Final report on the 2nd phase of development and testing of a horizontal axis wind turbine test rig for the investigation of stall regulation aerodynamics. Carried out under ETSU Agreement E.5A/CON5103/1746, April 1990.
- [15] Dular M, Bachert R, Sirok D, Stoffel B. Transient simulation, visualization and PIV-LIF measurements of the cavitation on different hydrofoil configurations. *Assn Mech Eng & Technicians of Slovenia. J Mech Eng* 2005;51(1):13–27.
- [16] Molland AF, Bahaj AS, Chaplin JR, Batten WMJ. Measurements and predictions of forces, pressures and cavitation on 2-D sections suitable for marine current turbines. *Proc Inst Mech Engrs M: J Eng Maritime Environ* 2004;218(2):127–38.